Eur. Phys. J. C (2022) 82:981
https://doi.org/10.1140/epjc/s10052-022-10926-5

THE EUROPEAN PHYSICAL JOURNAL C

Regular Article - Experimental Physics

Probing Higgs CP properties at the CEPC in the $e^+e^- \to ZH \to l^+l^-H$ using optimal variables

Qiyu Sha[1,a], **Abdualazem Fadol**[1,b], **Fangyi Guo**[1,c], **Gang Li**[1,d], **Yaquan Fang**[1,e], **Jiayin Gu**[2,3,f], **Xinchou Lou**[1,4,g]

[1] Institute of High Energy Physics, University of Chinese Academy of Sciences (CAS), 19B, Yuquan Road, Shijing District, Beijing 100049, China
[2] Department of Physics and Center for Field Theory and Particle Physics, Fudan University, Shanghai 200438, China
[3] Key Laboratory of Nuclear Physics and Ion-beam Application (MOE), Fudan University, Shanghai 200433, China
[4] University of Texas at Dallas, Richardson, TX 75080-3021, USA

Received: 2 August 2022 / Accepted: 15 October 2022

Abstract In the Circular Electron Positron Collider (CEPC), a measurement of the Higgs CP mixing through $e^+e^- \to ZH \to l^+l^-(e^+e^-/\mu^+\mu^-)H(\to b\bar{b}/c\bar{c}/gg)$ process is presented, with 5.6 ab^{-1} e^+e^- collision data at the center-of-mass energy of 240 GeV. In this study, the CP-violating parameter $\tilde{c}_{Z\gamma}$ is constrained between the region of -0.30 and 0.27 and $\tilde{c}_{ZZ}$ between -0.06 and 0.06 at 68% confidence level. This study demonstrates the great potential of probing Higgs CP properties at the CEPC.

1 Introduction

The historic discovery of Higgs boson with a mass around 125 GeV in 2012 by the ATLAS and CMS collaborations at the Large Hadron Collider (LHC) [1,2] completed the Standard Model (SM). This particle provides a new portal to search for new physics beyond the SM (BSM). The Higgs boson is predicted to be a scalar particle ($J^P = 0^{++}$) under the SM of particle physics. As a result, any observation of charge-parity violation (CPV) in Higgs would be a sign of physics BSM and could account for the explanation of the observed baryon asymmetry of the universe.

At present, the Higgs boson CP-mixing measurements are performed at hadron colliders. The hypothesis of spin-1 or spin-2 Higgs has been excluded by ATLAS and CMS at 99% confidence level (CL) with $\sqrt{s} = 7$ and 8 TeV, 25 fb^{-1} data [3]. Studies of the CP properties of the Higgs boson interactions with gauge bosons have been performed by the ATLAS [4–6] and CMS [7–9] experiments, and the results show no deviations from the SM predictions. ATLAS and CMS also finished analyses of $Ht\bar{t}$ coupling, which provides an alternative and independent avenue for CP testing in the Higgs sector because it is particularly sensitive to deviations from the SM coupling [10,11]; Their results show exclusion of the pure CP-odd structure of the top quark Yukawa ($t\bar{t}H$) coupling at 3.9σ (3.2σ) and the fractional contribution of the CP-odd component is measured to be $f_{CP}^{Ht\bar{t}} = 0.00 \pm 0.33$.

However, small anomalous contributions were not excluded. At the HL-LHC [12], the CP-odd VVH couplings are introduced and the expected results constrain the CP-odd parameters $\tilde{c}_{Z\gamma}$ between -0.22 and 0.22 and the $\tilde{c}_{ZZ}$ between -0.33 and 0.33 at the 68% confidence level.

In terms of probing the CP-odd Higgs couplings, a lepton collider operating as a Higgs factory has great advantages, as it is free of the QCD background and has tunable and precisely defined initial energies. Several future lepton colliders, including the International Linear Collider (ILC) [13], the e^+e^- Future Circular Collider (FCC-ee) [14], the Compact Linear Collider (CLIC) [15], and the Circular Electron-Positron Collider (CEPC) [16], have been proposed with the capability of precise measurement of Higgs boson parameters. There are plenty of approaches to the Higgs CP measurements at the future lepton colliders by using different probes, like the VH process, the $t\bar{t}H$ process, the VBF

[a] e-mail: shaqiyu@ihep.ac.cn (corresponding author)
[b] e-mail: amohammed@aims.ac.tz
[c] e-mail: guofangyi@ihep.ac.cn
[d] e-mail: li.gang@ihep.ac.cn
[e] e-mail: fangyq@ihep.ac.cn
[f] e-mail: jiayin_gu@fudan.edu.cn
[g] e-mail: xinchou@ihep.ac.cn

Published online: 01 November 2022

process and the $H \to \tau^+\tau^-$ process [17]. For example, the VBF process, an ongoing study of the Z-fusion process at 1.4 TeV CLIC and 1 TeV ILC are mentioned in Ref [18]. For the past CP-odd VVH couplings studies, at the ILC [19], the CP-mixing angle of τ pair from Higgs boson decays can reach an accuracy of 4.3° with 2 ab^{-1} of polarized data at 250 GeV [18,20] and the anomalous couplings b_Z and $\tilde{b}_Z$ with the new Lorentz structures can reach $< 1\%$ [21]. The best 95% CL limits at the loose working point (90% b-tagging efficiency) on CP-violating couplings $\tilde{c}_{HW}$ and $\tilde{c}_{HB}$ are $\left[-7.0\times10^{-3}, 7.0\times10^{-3}\right]$ and $\left[-3.0\times10^{-2}, 3.0\times10^{-2}\right]$, respectively at the 3 TeV energy stage of CLIC [22] via the $e^+e^- \to \nu\bar{\nu}H$ process. The CP violation parameter $\tilde{g}$ can reach the limit of $[-0.04, 0.01]$ at the CEPC [23] which is similar to this letter, but the current study obtain a better result after using full simulation and the technique of optimal observable. As for the past CP study at the future linear e^+e^- colliders (including ILC at 500 GeV and CLIC at 380 GeV) [24], their results show the potential of measuring CP violation in the top-quark sector at future e^+e^- collider.

The CEPC will operate at a center-of-mass energy of $\sqrt{s} \sim 240$ GeV which is close to the maximum of the Higgs boson production cross-section through the $e^+e^- \to ZH$ process. Over one million Higgs bosons with an integrated luminosity of 5.6 ab^{-1} will be produced. In comparison to the LHC, the cleaner environment of the CEPC allows significantly better exclusive measurements of Higgs boson decay channels. So, in the future, more precise Higgs-gauge boson coupling studies can be performed, such as this Higgs CP measurement through $e^+e^- \to ZH \to (e^+e^-/\mu^+\mu^-)H(\to b\bar{b}/c\bar{c}/gg)$ process [25].

This letter is organized as follows: in Sect. 2, we introduces the theory framework for the analysis of Higgs CP-mixing. The MC samples and event selections are described in Sects. 3 and 4 respectively. Section 5 describes the strategy for analysis and interprets the results of this study. The conclusions are presented in Sect. 7.

2 Theory framework

To parametrize BSM effects in a general way, we assume that the new physics sector is characterized by a scale Λ, which is significantly higher than the electroweak scale, and the SM is supplemented with 59 independent dimension-6 operators [26]. This Lagrangian can be schematically cast as:

$$\mathcal{L}_{\text{eff}} = \mathcal{L}^{(4)}_{\text{SM}} + \frac{1}{\Lambda^2}\sum_{k=1}^{59}\alpha_k\mathcal{O}_k, \tag{1}$$

where the α_k is the coupling of operator $\mathcal{O}_k$. Apart from the SM tree contributions, we only consider effects of order $1/\Lambda^2$ on the decay amplitude. In the broken-symmetry phase, the effective Lagrangian Eq. (1) generates the terms [27] [28]:

$$\begin{aligned}\mathcal{L}_{\text{eff}} \supset & c^{(1)}_{ZZ} H Z_\mu Z^\mu + c^{(2)}_{ZZ} H Z_{\mu\nu} Z^{\mu\nu} + c_{Z\tilde{Z}} H Z_{\mu\nu}\tilde{Z}^{\mu\nu} \\ & + c_{AZ} H Z_{\mu\nu} A^{\mu\nu} + c_{A\tilde{Z}} H Z_{\mu\nu}\tilde{A}^{\mu\nu} \\ & + H Z_\mu \bar{\ell}\gamma^\mu \left(c_V + c_A\gamma_5\right)\ell + Z_\mu \bar{\ell}\gamma^\mu\left(g_V - g_A\gamma_5\right)\ell \\ & - g_{\text{em}} Q_\ell A_\mu \bar{\ell}\gamma^\mu \ell,\end{aligned} \tag{2}$$

which includes the relevant tree-level SM terms. The Higgs-gauge couplings of Eq. (2) are given by

$$\begin{aligned} c^{(1)}_{ZZ} &= m_Z^2\left(\sqrt{2}G_F\right)^{1/2}\left(1+\hat{\alpha}^{(1)}_{ZZ}\right), \\ c^{(2)}_{ZZ} &= \left(\sqrt{2}G_F\right)^{1/2}\hat{\alpha}_{ZZ}, \\ c_{Z\tilde{Z}} &= \left(\sqrt{2}G_F\right)^{1/2}\hat{\alpha}_{Z\tilde{Z}}, \\ c_{AZ} &= \left(\sqrt{2}G_F\right)^{1/2}\hat{\alpha}_{AZ}, \\ c_{A\tilde{Z}} &= \left(\sqrt{2}G_F\right)^{1/2}\hat{\alpha}_{A\tilde{Z}}, \end{aligned} \tag{3}$$

where the $\hat{\alpha}_{A\tilde{Z}}$ and $\hat{\alpha}_{Z\tilde{Z}}$ are CP-violation parameters.

The differential cross-section for $e^+e^- \to ZH \to l^+l^-H(\to b\bar{b}/c\bar{c}/gg)$ is given by:

$$\frac{\mathrm{d}\sigma}{\mathrm{d}\cos\theta_1 \mathrm{d}\cos\theta_2\,\mathrm{d}\psi} = \frac{1}{m_H^2}\mathcal{N}_\sigma\left(q^2\right)\mathcal{J}\left(q^2,\theta_1,\theta_2,\phi\right), \tag{4}$$

where the definitions of three angles are shown in Appendix A. $\mathcal{N}_\sigma\left(q^2\right)$ is the normalization factor and it can be written in terms of the dimensionless parameters r and s as:

$$\mathcal{N}_\sigma\left(q^2\right) = \frac{1}{2^{10}(2\pi)^3}\frac{1}{\sqrt{r}\,\gamma\,Z}\frac{\sqrt{\lambda(1,s,r)}}{s^2}, \tag{5}$$

where λ is the källén functions and, the constant dimensionless parameters are given by the following:

$$s = \frac{q^2_{\text{th}}}{m_H^2} \approx 3.68, r = \frac{m_Z^2}{m_H^2} \approx 0.53, \gamma Z = \frac{\Gamma_Z}{m_H} \approx 0.020. \tag{6}$$

$\mathcal{J}$ can be expressed by:

$$\begin{aligned}\mathcal{J}\left(q^2,\theta_1,\theta_2,\phi\right) = & J_1\left(1+\cos^2\theta_1\cos^2\theta_2+\cos^2\theta_1+\cos^2\theta_2\right) \\ & + J_2\sin^2\theta_1\sin^2\theta_2 + J_3\cos\theta_1\cos\theta_2 \\ & + \left(J_4\sin\theta_1\sin\theta_2 + J_5\sin 2\theta_1\sin 2\theta_2\right)\sin\phi \\ & + \left(J_6\sin\theta_1\sin\theta_2 + J_7\sin 2\theta_1\sin 2\theta_2\right)\cos\phi \\ & + J_8\sin^2\theta_1\sin^2\theta_2\sin 2\phi\end{aligned}$$

$$+J_9 \sin^2\theta_1 \sin^2\theta_2 \cos 2\phi, \tag{7}$$

where the explicit form of the J_i in terms of the EFT coefficients and Standard Model parameters was computed by the authors of [27] and for convenience is given in Appendix B.

Among all the BSM variables, only $\hat{\alpha}_{A\tilde{Z}}$ and $\hat{\alpha}_{Z\tilde{Z}}$, shown in Eq. (B2), contribute to the *CP*-odd. So those are the *CP*-violating parameters that we need to study.

In addition to simplify the analysis, we only constrain the CP-violating parameters with the assumption that all other parameters are zero. Three of the J_i functions shown in Eq. (B1), namely J_4, J_5, J_8, are *CP*-odd and vanish in the SM at tree level, whereas the remaining six functions are *CP*-even. As a result, the differential cross-section can be represented as follows:

$$\frac{d\sigma}{d\cos\theta_1 d\cos\theta_2 d\phi} = N \times \left(J_{even}(\theta_1,\theta_2,\phi) + \hat{\alpha}_{A\tilde{Z}} \times J_{odd_1}(\theta_1,\theta_2,\phi) + \hat{\alpha}_{Z\tilde{Z}} \times J_{odd_2}(\theta_1,\theta_2,\phi)\right), \tag{8}$$

where J_{odd_1} and J_{odd_2} are part of J_{odd}.

Two optimal variables combining the information from $\{\theta_1, \theta_2, \phi\}$ can be defined as following:

$$\omega_1 = \frac{J_{odd_1}(\theta_1,\theta_2,\phi)}{J_{even}(\theta_1,\theta_2,\phi)}, \tag{9}$$

$$\omega_2 = \frac{J_{odd_2}(\theta_1,\theta_2,\phi)}{J_{even}(\theta_1,\theta_2,\phi)}, \tag{10}$$

where ω_1 and ω_2 combine the information from 3-dimension phase space and can be used to measure $\hat{\alpha}_{A\tilde{Z}}$ and $\hat{\alpha}_{Z\tilde{Z}}$, respectively.

It is an optimal use of the complete information from the decay as it is more convenient and efficient than using the full multi-dimensional distribution, as shown in [29]. Therefore, we can use the one-dimensional distribution of the single variable ω to substitute the multi-dimensional distribution without any loss of information. Furthermore, it can help us improve the result compared to the one in Ref. [23] which only uses the ϕ information.

The parametric curves with different $\hat{\alpha}_{A\tilde{Z}}$ values are shown in Fig. 1 and with different $\hat{\alpha}_{Z\tilde{Z}}$ values in Fig. 2.

3 Monte Carlo samples

The SM Higgs and background samples, generated with Whizard 1.95 [30] and fully simulated with the CEPC baseline [16] detector design, are used to calculate the selection efficiencies and study background. The details of the event generation can be found at Ref. [31]. Moreover, CP-mixing Higgs samples are generated according to Eq. (1). The study assumes that $\sqrt{s}$ is 240 GeV. The mass of the Higgs boson is set to be 125 GeV. All the generations are normalized to the expected yields with an integrated luminosity of 5.6 ab^{-1}.

4 Event selection

The signal sample is the process of $e^+e^- \to ZH \to l^+l^-H(\to b\bar{b}/c\bar{c}/gg)$, containing two jets and two leptons with opposite charges in the final state. Only irreducible backgrounds are considered in the study, mainly $e^+e^- \to ZZ \to l^+l^-q\bar{q}$ because that the reducible background has very little contribution according to a previous study [32].

Each event must contain two isolated tracks with opposite charges, reconstructed as e^+e^- or $\mu^+\mu^-$ .The energy of each isolated lepton candidate must be above 20 GeV. The polar angle of the muon pair system is required to be in the range of $\left|\cos\theta_{\mu^+\mu^-}\right| < 0.81$. The invariant mass of the muon pair must be within the Z mass window, which is defined as from 77.5 GeV to 104.5 GeV. The invariant mass of the muon pair's recoil system, denoted as $M^{\mu^+\mu^-}_{\text{recoil}}$, can provide a clear signature of the $\mu\mu H$ events. The definition of $M^{\mu^+\mu^-}_{\text{recoil}}$ is:

$$\begin{aligned} M^{\mu^+\mu^-}_{\text{recoil}} &= \sqrt{\left(\sqrt{s} - E_{\mu^+\mu^-}\right)^2 - p^2_{\mu^+\mu^-}} \\ &= \sqrt{s - 2E_{\mu^+\mu^-}\sqrt{s} + m^2_{\mu^+\mu^-}}, \end{aligned} \tag{11}$$

in which $\sqrt{s} = 240$ GeV, and $E_{\mu\mu}$ and $m_{\mu\mu}$ stand for the energy and mass of the muons, respectively. A Higgs mass window is defined by requiring $M^{\mu^+\mu^-}_{\text{recoil}}$ between 124 GeV and 140 GeV.

The remaining particles in the event are used to reconstruct exactly two jets with a polar angle θ_{jet} in the range of $\left|\cos\theta_{\text{jet}}\right| < 0.96$, using *ee*-kt algorithm [33]. The invariant mass of the pair of jets is required to be between 100 GeV and 150 GeV to reject the background.

Compared to the analysis of the $ZH \to \mu^+\mu^-H$ decay, the analysis of the $ZH \to e^+e^-H$ decay suffers from large background. A cut based event selection is performed for the $ZH \to e^+e^-H$ process. The electron-positron pair is required to have its invariant mass in the range of 85−95 GeV and the polar angle of each electron is required to satisfy $|\cos\phi_e| < 0.95$. The other selection criteria are same as $\mu^+\mu^-H$ analysis. It should be noticed that the effect of Z-fusion in e^+e^-H process is neglected in this study since its cross section is rather small.

The expected signal and background yields during the event selections are summarized in Table 1 for $\mu^+\mu^-H$ and e^+e^-H analysis, respectively.

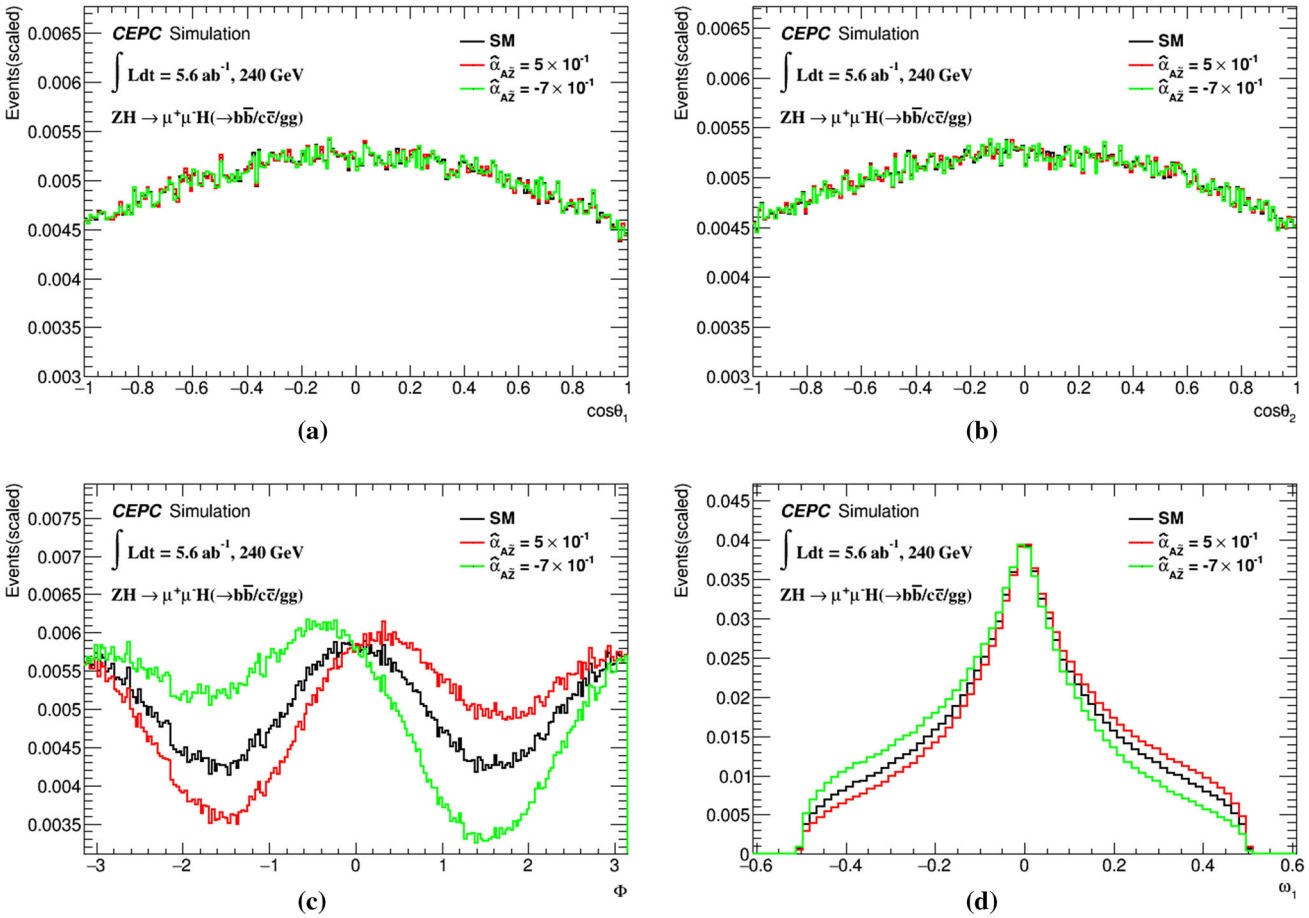

Fig. 1 Parametric curves with different $\hat{\alpha}_{A\tilde{Z}}$ values. The optimal variable ω_1 is defined in the text. (The value of ω_1 here is multiplied by 1000 for numerical convenience.)

5 Fitting strategy and result

After the event selections, the correlations among $(\theta_1, \theta_2, \phi)$ and the variables for selection, such as $\cos\theta_{l^+l^-}$, $\text{Mass}_{l^+l^-}$, $M^{l^+l^-}_{\text{recoil}}$, $\cos\theta_{\text{jet}}$, Mass_{jj}, are carefully investigated and the impacts on CP study are negligible.

5.1 $\mu^+\mu^- H$ results obtained by ω-fitting

The CP-violating parameters $\hat{\alpha}_{A\tilde{Z}}$ and $\hat{\alpha}_{Z\tilde{Z}}$ can be measured through the optimal variable ω_1 and ω_2. The estimation of $\hat{\alpha}_{A\tilde{Z}}$ and $\hat{\alpha}_{Z\tilde{Z}}$ uses a maximum-likelihood fit which could be constructed as:

$$\mathcal{L}(\vec{x} \mid \vec{\alpha}) = \prod_{\text{data}} f\left(x_i \mid \vec{\alpha}\right), \tag{12}$$

where $\vec{\alpha}$ are CP-violating parameters ($\hat{\alpha}_{A\tilde{Z}}$ and $\hat{\alpha}_{Z\tilde{Z}}$) to be estimated, and x is the dataset. For each $\vec{\alpha}$ hypothesis, the profile of a negative log-likelihood (NLL) is calculated. The best-estimated $\vec{\alpha}$, as well as its central confidence interval at a 68% (95%) confidence level (CL), can be determined at $\Delta NLL = NLL - NLL_{\text{min}} = 0.5$ (1.96).

The main sensitive variable for the CP test in this analysis is the optimal variable ω (stand for ω_1 and ω_2), which combines all 3 kinematic variables of θ_1, θ_2, and ϕ, and the function used to determine the $\vec{\alpha}$-value can be defined as:

$$f^{\vec{\alpha}}(\omega) = N_{\text{sig}} * f^{\vec{\alpha}}_{\text{sig}}(\omega) + N_{bkg} * f^{\vec{\alpha}}_{bkg}(\omega), \tag{13}$$

where $f^{\vec{\alpha}}_{\text{sig}}(\omega)$ and $f^{\vec{\alpha}}_{\text{bkg}}(\omega)$ are probability density functions (PDFs) of the signal and background, and N_{sig} and N_{bkg} are the yields of them, respectively.

For the modeling of signal, PDFs are generated according to different $\vec{\alpha}$ hypothesises, and background PDF is fixed to the MC simulation. The $M^{\mu^+\mu^-}_{\text{recoil}}$ distribution is essential to discriminate signal over background. The background, dominated by the $e^+e^- \to ZZ \to \mu^+\mu^- q\bar{q}$, is modeled by a second-order polynomial, while the signal is modeled by the Crystal Ball function [34]. Figure 3 shows the fit result of ω and $M^{\mu^+\mu^-}_{\text{recoil}}$.

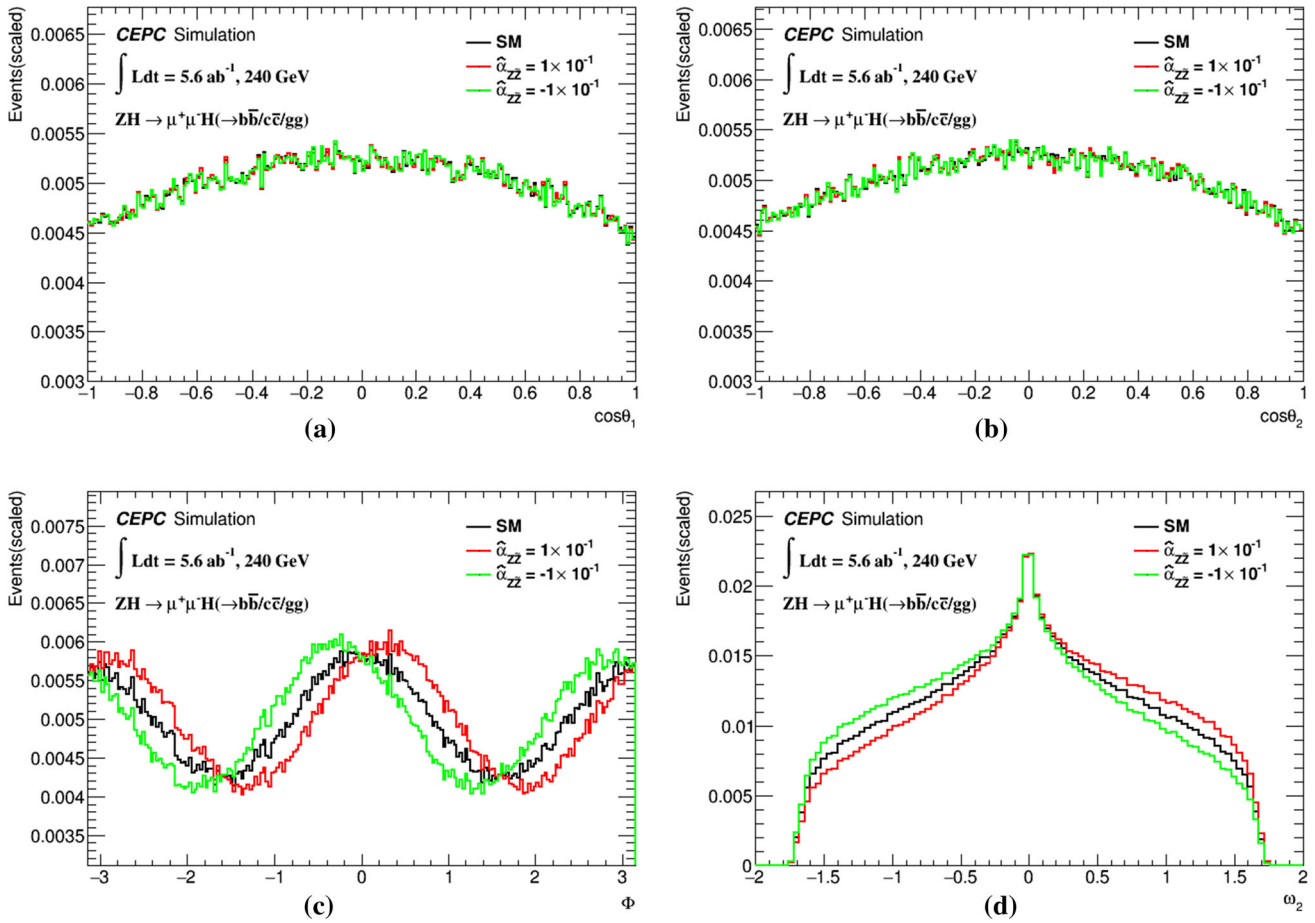

Fig. 2 Parametric curves with different $\hat{\alpha}_{Z\tilde{Z}}$ values. The optimal variable ω_2 is defined in the text. (The value of ω_2 here is multiplied by 1000 for numerical convenience.)

Table 1 Event yields of cut flow. Signal events are $ZH \to l^+l^-H$, $H \to b\bar{b}/c\bar{c}/gg$ combined. Background is the $e^+e^-/\mu^+\mu^-$+jet pair process.

	Signal	Background
$ZH \to \mu^+\mu^-H(\to b\bar{b}/c\bar{c}/gg)$ channel		
Original	2.62×10^4	1.25×10^6
Leptonn pair selection	1.59×10^4	9.91×10^3
All selection	1.48×10^4	5.60×10^3
$ZH \to e^+e^-H(\to b\bar{b}/c\bar{c}/gg)$ channel		
Original	2.72×10^4	1.77×10^6
Lepton pair selection	8.76×10^3	8.77×10^4
All selection	7.15×10^3	4.59×10^3

The individual fitting with each single CPV parameter has been performed by assuming $\widehat{\alpha}_{A\tilde{Z}}$ is a free parameter with $\widehat{\alpha}_{Z\tilde{Z}} = 0$ and vice versa. The expected and observed ΔNLL curves are shown in Fig. 4 as a quadratic function of $\vec{\alpha}$. It corresponds to the SM prediction that $\vec{\alpha}$ equals to zero, and the results of $\widehat{\alpha}_{Z\tilde{Z}}$ and $\hat{\alpha}_{A\tilde{Z}}$ with confidence interval at 68% (95%) represent the sensitivity to a CP-odd Higgs, which are shown in Table 2.

5.2 $\mu^+\mu^-H$ results obtained by ϕ-fitting

Because the ϕ contains the most information among the three kinematic variables, it is straightforward and feasible to fit to ϕ.

Similar to the Eq. (13), the function used to obtain the $\vec{\alpha}$ is as following:

$$f^{\vec{\alpha}}(\phi) = N_{\text{sig}} * f^{\vec{\alpha}}_{\text{sig}}(\phi) + N_{bkg} * f^{\vec{\alpha}}_{bkg}(\phi), \tag{14}$$

where the definitions of $f^{\vec{\alpha}}_{\text{sig}}(\phi)$, $f^{\vec{\alpha}}_{\text{bkg}}(\phi)$, N_{sig} and N_{bkg} are the same as those used to fit to ω above.

After fitting with a single CPV parameter, the fit results are shown in Fig. 5, the ΔNLL curves in Fig. 6.

The comparison with the results of ω-fitting is shown in Table 2. It can be seen that the results of the ϕ-fitting is slightly worse than those of the ω-fitting as expected, since fewer kinematic variables, i.e, less information, are used.

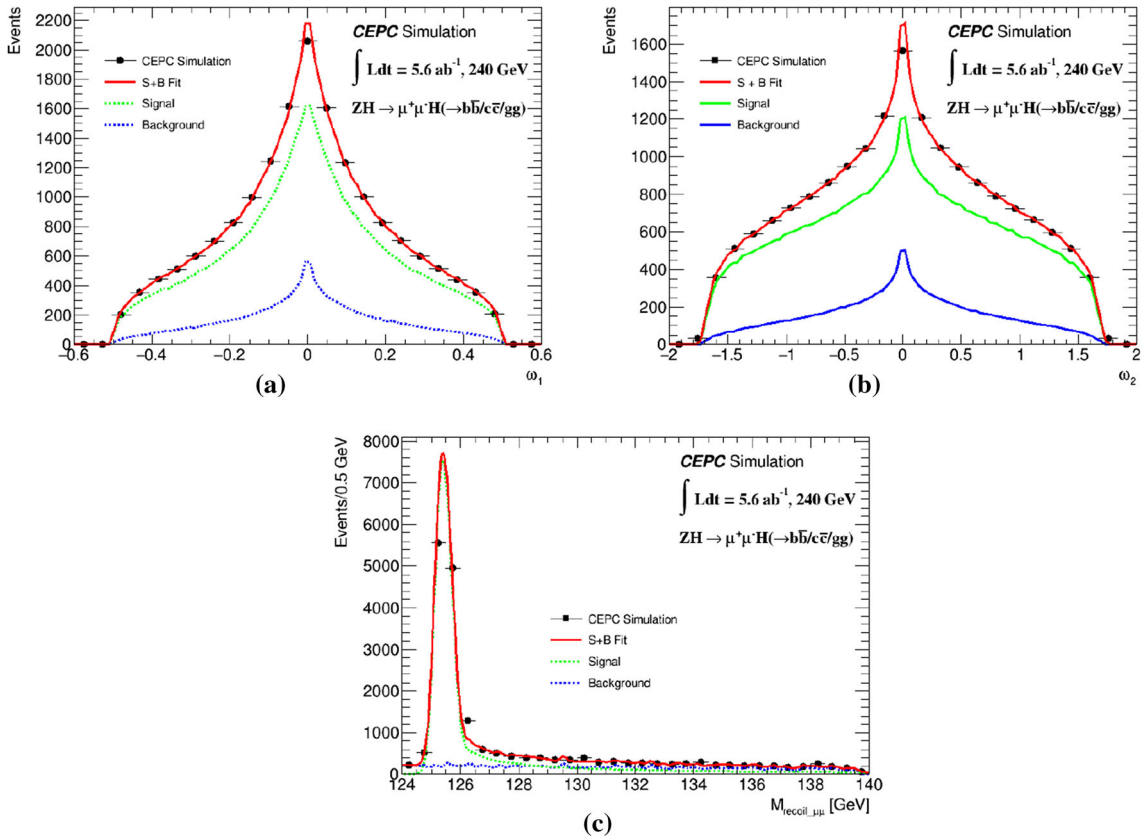

Fig. 3 **a** Fit result projected on ω_1 distribution in $\mu^+\mu^- H$ channel, **b** fit result projected on ω_2 distribution in $\mu^+\mu^- H$ channel, **c** fit result projected on recoil mass distribution in $\mu^+\mu^- H$ channel

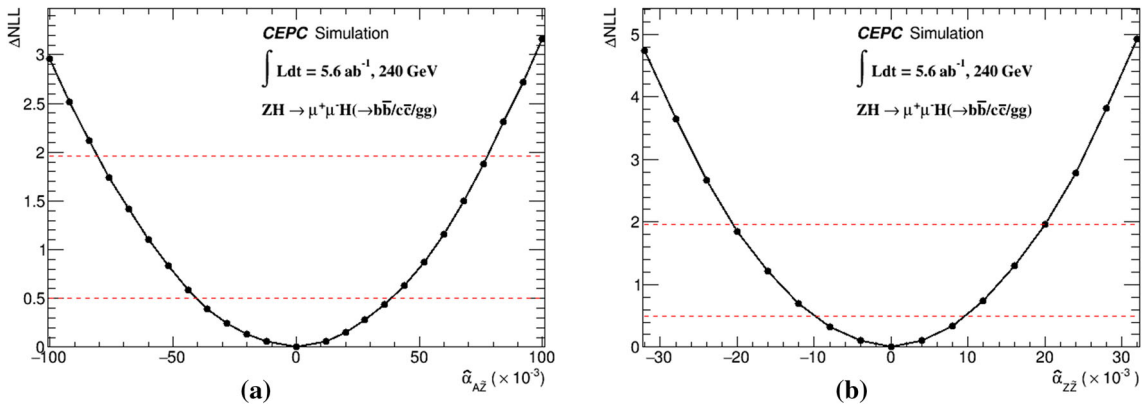

Fig. 4 **a** ΔNLL curve (fit to $\hat{\alpha}_{A\tilde{Z}}$ with $\widehat{\alpha}_{Z\tilde{Z}} = 0$), **b** ΔNLL curve (fit to $\hat{\alpha}_{Z\tilde{Z}}$ with $\widehat{\alpha}_{A\tilde{Z}} = 0$)

5.3 Combined results obtained by ω-fitting

By using the same process shown in Sect. 5.1, the $e^+e^- H$ results with ω-fitting can be easy obtained. Neglecting the migration between $e^+e^- H$ and $\mu^+\mu^- H$, the combined likelihood is equal to the multiplication of the likelihood of $e^+e^- H$ and $\mu^+\mu^- H$ channels.

According to the latest note [35], CEPC Higgs operation can be upgraded to 20 ab^{-1}. With this increasing luminosity, the updated numerical results after applying the conversion which is described in Sect. 6 are shown in Table 4. This result is about two times better than that of 5.6 ab^{-1}.

6 Discussion

Because studies of different CP-odd VVH coupling use different symbols or methods, this makes it difficult to visually

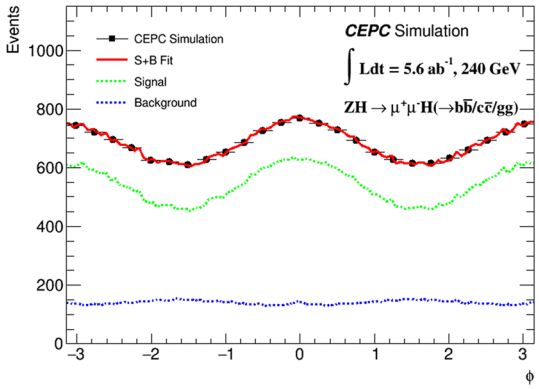

Fig. 5 Fit result projected on ϕ distribution in $\mu^+\mu^- H$ channel

Table 2 Summary of 1σ and 2σ bounds on $\hat{\alpha}_{A\tilde{Z}}$ and $\hat{\alpha}_{Z\tilde{Z}}$ from various analyses by fitting to ϕ and fitting to ω through $\mu^+\mu^- H$ process which is shown in Sects. 5.1 and 5.2.

	$\hat{\alpha}_{A\tilde{Z}}(\times 10^{-2})$	$\hat{\alpha}_{Z\tilde{Z}}(\times 10^{-2})$
	ω-fitting	
68% CL(1σ)	$[-4.16, 3.88]$	$[-1.06, 1.00]$
95% CL(2σ)	$[-8.10, 7.82]$	$[-2.06, 2.01]$
	ϕ-fitting	
68% CL(1σ)	$[-4.42, 4.21]$	$[-1.35, 1.24]$
95% CL(2σ)	$[-8.66, 8.45]$	$[-2.62, 2.51]$

compare results with each other. In order to compare with other analysis introduced in the Sect. 1, it is necessary to do some conversion.

For HL-LHC [12]. The CPV Lagrangian which HL-LHC used is given by:

$$\mathcal{L}_{\rm CPV} = \frac{H}{v}\left[\tilde{c}_{\gamma\gamma}\frac{e^2}{4}A_{\mu\nu}\tilde{A}^{\mu\nu} + \tilde{c}_{Z\gamma}\frac{e\sqrt{g_1^2+g_2^2}}{2}Z_{\mu\nu}\tilde{A}^{\mu\nu} + \tilde{c}_{ZZ}\frac{g_1^2+g_2^2}{4}Z_{\mu\nu}\tilde{Z}^{\mu\nu} + \tilde{c}_{WW}\frac{g_2^2}{2}W^+_{\mu\nu}\tilde{W}^{-\mu\nu}\right], \quad (15)$$

where g_1 and g_2 are the $U(1)_Y$ and $SU(2)_L$ gauge coupling constants.

Comparing Eqs. (15) and (2), the connections of the *CP*-odd related parameters between the two equations are obvious,

$$\left(\sqrt{2}G_F\right)^{1/2}\hat{\alpha}_{ZZ}HZ_{\mu\nu}\tilde{Z}^{\mu\nu} = \frac{H}{v}\tilde{c}_{ZZ}\frac{g_1^2+g_2^2}{4}Z_{\mu\nu}\tilde{Z}^{\mu\nu},$$
$$\left(\sqrt{2}G_F\right)^{1/2}\hat{\alpha}_{A\tilde{Z}}HZ_{\mu\nu}\tilde{A}^{\mu\nu} = \frac{H}{v}\tilde{c}_{Z\gamma}\frac{e\sqrt{g_1^2+g_2^2}}{2}Z_{\mu\nu}\tilde{A}^{\mu\nu}, \quad (16)$$

where g_1 and g_2 equal to 0.358 and 0.648, respectively, $v = (\sqrt{2}G_F)^{-1/2} = 2M_W/g$, and e is the EM coupling which equals to 0.313.

Converted with the Eq. (16), all the results are summarized in Table 3. The 1σ bounds on $\tilde{c}_{Z_\gamma}$ and $\tilde{c}_{ZZ}$ are $[-0.30, 0.27]$ and $[-0.06, 0.06]$ respectively. These results are significantly better than HL-LHC on the $\tilde{c}_{ZZ}$ and comparable on the $\tilde{c}_{Z\gamma}$ due to a cleaner environment and higher luminosity in CEPC.

We use the *CP*-violation variables $\tilde{c}_{Z_\gamma}$ and $\tilde{c}_{ZZ}$ which are used by HL-LHC as a benchmark. After similar conversions which are shown in the Appendix C, we can get transformed results of other analysis.

For the previous CEPC CP study [23], the CP violation parameter $\tilde{g}$ can reach the limit of $[-0.04, 0.01]$, it means the 1σ bounds on $\tilde{c}_{ZZ}$ is $[-0.20, 0.05]$ after converting with the Eq. (C2). Our study achieves a better result than this previous study because that the technique of optimal observable makes use of the complete kinematics information.

Also, converted with the Eq. (C5), the 2σ bounds on $\tilde{c}_{Z_\gamma}$ and $\tilde{c}_{ZZ}$ are $[-0.36, 0.36]$ and $[-0.24, 0.24]$ respectively in CLIC study [22]. Assuming that their constraints are in the interference term, it can be approximated that the 1σ bounds on $\tilde{c}_{Z_\gamma}$ and $\tilde{c}_{ZZ}$ are $[-0.18, 0.18]$ and $[-0.12, 0.12]$. This

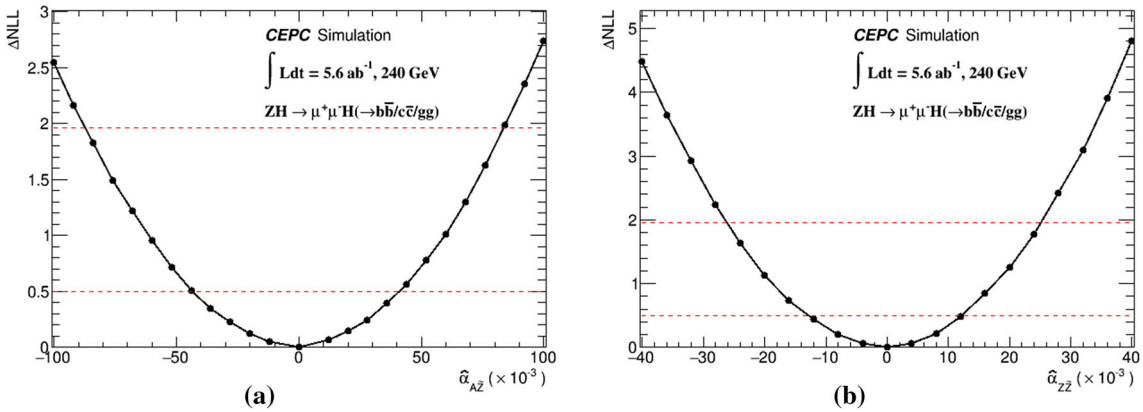

Fig. 6 **a** ΔNLL curve (fit to $\hat{\alpha}_{A\tilde{Z}}$ with $\hat{\alpha}_{Z\tilde{Z}} = 0$), **b** ΔNLL curve (fit to $\hat{\alpha}_{Z\tilde{Z}}$ with $\hat{\alpha}_{A\tilde{Z}} = 0$)

Table 3 Summary of 1σ bounds on $\tilde{c}_{Z\gamma}$ and $\tilde{c}_{ZZ}$ from various analyses considered in our study, HL-LHC analysis, and CLIC analysis

Collider	pp	e^+e^-	e^+e^-	e^+e^-
E (GeV)	14,000	3000	240	240
$\mathcal{L}\,(\text{fb}^{-1})$	3000	5000	5600	20,000
$\tilde{c}_{Z\gamma}\ (1\sigma)$	$[-0.22, 0.22]$	$[-0.18, 0.18]$	$[-0.30, 0.27]$	$[-0.16, 0.14]$
$\tilde{c}_{ZZ}\ (1\sigma)$	$[-0.33, 0.33]$	$[-0.12, 0.12]$	$[-0.06, 0.06]$	$[-0.03, 0.03]$

Table 4 Summary of 1σ and 2σ bounds on CP-violating parameters $\tilde{c}_{Z\gamma}$, $\tilde{c}_{ZZ}$ from various analyses considered in our study with different channels by fitting to ω with 5.6 ab^{-1} and 20 ab^{-1}

	5.6 ab^{-1}		20 ab^{-1}	
	$\tilde{c}_{Z\gamma}$	$\tilde{c}_{ZZ}$	$\tilde{c}_{Z\gamma}$	$\tilde{c}_{ZZ}$
	$\mu^+\mu^- H$ channel			
68% CL(1σ)	$[-0.36, 0.33]$	$[-0.08, 0.07]$	$[-0.19, 0.17]$	$[-0.04, 0.04]$
95% CL(2σ)	$[-0.70, 0.67]$	$[-0.15, 0.15]$	$[-0.37, 0.35]$	$[-0.08, 0.08]$
	$e^+e^- H$ channel			
68% CL(1σ)	$[-0.51, 0.47]$	$[-0.11, 0.11]$	$[-0.28, 0.24]$	$[-0.06, 0.06]$
95% CL(2σ)	$[-1.00, 0.95]$	$[-0.21, 0.21]$	$[-0.53, 0.49]$	$[-0.11, 0.11]$
	Combined results			
68% CL(1σ)	$[-0.30, 0.27]$	$[-0.06, 0.06]$	$[-0.16, 0.14]$	$[-0.03, 0.03]$
95% CL(2σ)	$[-0.58, 0.55]$	$[-0.12, 0.12]$	$[-0.31, 0.28]$	$[-0.06, 0.06]$

result is comparable to us as expected and the comparison is shown in Table 3.

7 Conclusion

In summary, the Higgs CP is studied by analyzing the $e^+e^- \to ZH \to (\mu^+\mu^-/e^+e^-)H(\to b\bar{b}/c\bar{c}/gg)$ process in a 5.6 ab^{-1} e^+e^- collision sample with $\sqrt{s} = 240$ GeV at the CEPC. The simplest CP mixing model and two optimal variables combining three related kinematic variables are used in this analysis and show very promising sensitivity (Table 4). The optimal variables improve results compared to just using the angular distribution between the H and Z decay-planes. The CP-violating parameter $\tilde{c}_{Z\gamma}$ is determined to be greater (less) than 0.30 (-0.27) and $\tilde{c}_{ZZ}$ greater (less) than 0.06 (-0.06) at 95% confidence level. Considering possibly the increasing luminosity such as 20 ab^{-1}, the sensitivities to new physics could be further improved, The CP-violating parameter $\tilde{c}_{Z\gamma}$ is determined to be greater (less) than 0.16 (-0.14) and $\tilde{c}_{ZZ}$ greater (less) than 0.03 (-0.03) at 68% confidence level. In the $\tilde{c}_{ZZ}$ part, there is an order of magnitude improvement over the HL-LHC.

Acknowledgements This study is supported by National Natural Science Foundation of China (NSFC) under Grant No. 12035008 and No.12075271, the Innovation fundation of IHEP under Grant No. E2545AU210.

Data Availability Statement This manuscript has no associated data or the data will not be deposited. [Authors' comment: Anyone who need the raw data can contact the corresponding author.]

Funded by SCOAP[3]. SCOAP[3] supports the goals of the International Year of Basic Sciences for Sustainable Development.

Appendix A

Here we describe the angle conventions used in our results. Using the conventions for the axes giving in Fig. 7. We choose the direction z direction to be defined by the momentum of the on-shell Z boson in the e^+e^- state rest frame. The θ_1 is the angle between the momentum of ℓ^-, and the z axis. The angle θ_2^- is the angle between the direction pf flight of the e^- and the z axis in the e^+e^- rest frame. To best exploit the crossing symmetry of the two processes, one should describe the reaction using the angle θ_2^+ measured from the z axis to

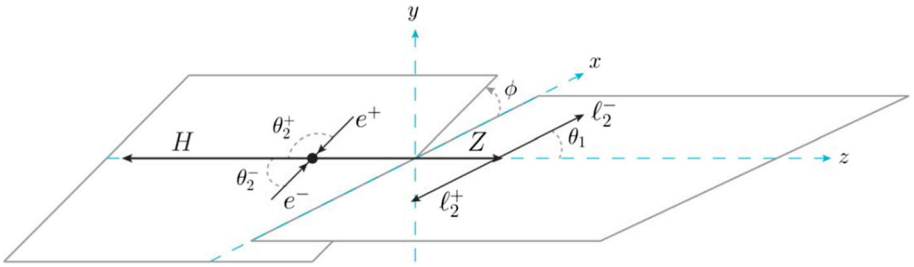

Fig. 7 Kinematics for the scattering $e^+e^- \to ZH \to l^+l^-$ [27]

the direction of flight of the e^+. Our Eq. 4 are therefore written in terms of the angle:

$$\theta_2^+ \equiv \theta_2 = \pi - \theta_2^-. \tag{A1}$$

Also ϕ is the angle between the normal of the planes defined by the z direction and the momenta of ℓ^- and e^-. It is measured positively from the $\ell^+\ell^-$ plane to the e^+e^- plane.

Appendix B

For completeness, here we list the various J_i coefficients computed first in [27]. These coefficients are conveniently expressed in terms of components of the matrix element as

$$\begin{aligned}
J_1 &= 2\,r\,s\left(g_A^2+g_V^2\right)\left(\left|H_{1,V}\right|^2+\left|H_{1,A}\right|^2\right),\\
J_2 &= \kappa\left(g_A^2+g_V^2\right)\\
&\left[\kappa\left(\left|H_{1,V}\right|^2+\left|H_{1,A}\right|^2\right)+\lambda\,\mathrm{Re}\left(H_{1,V}\,H_{2,V}^*+H_{1,A}\,H_{2,A}^*\right)\right],\\
J_3 &= 32r\,s\,g_A\,g_V\,\mathrm{Re}\left(H_{1,V}\,H_{1,A}^*\right),\\
J_4 &= 4\kappa\sqrt{r\,s\,\lambda}\,g_A\,g_V\,\mathrm{Re}\left(H_{1,V}\,H_{3,A}^*+H_{1,A}\,H_{3,V}^*\right),\\
J_5 &= \frac{1}{2}\kappa\sqrt{r\,s\,\lambda}\left(g_A^2+g_V^2\right)\mathrm{Re}\left(H_{1,V}\,H_{3,V}^*+H_{1,A}\,H_{3,A}^*\right),\\
J_6 &= 4\sqrt{r\,s}\,g_A\,g_V\left[4\kappa\,\mathrm{Re}\left(H_{1,V}\,H_{1,A}^*\right)\right.\\
&\left.+\lambda\,\mathrm{Re}\left(H_{1,V}\,H_{2,A}^*+H_{1,A}\,H_{2,V}^*\right)\right],\\
J_7 &= \frac{1}{2}\sqrt{r\,s}\left(g_A^2+g_V^2\right)\\
&\left[2\kappa\left(\left|H_{1,V}\right|^2+\left|H_{1,A}\right|^2\right)+\lambda\,\mathrm{Re}\left(H_{1,V}\,H_{2,V}^*+H_{1,A}\,H_{2,A}^*\right)\right],\\
J_8 &= 2\,r\,s\sqrt{\lambda}\left(g_A^2+g_V^2\right)\mathrm{Re}\left(H_{1,V}\,H_{3,V}^*+H_{1,A}\,H_{3,A}^*\right),\\
J_9 &= 2\,r\,s\left(g_A^2+g_V^2\right)\left(\left|H_{1,V}\right|^2+\left|H_{1,A}\right|^2\right).
\end{aligned} \tag{B1}$$

The expressions for $H_{i,V/A}$ at $\mathcal{O}\left(1/\Lambda^2\right)$ are:

$$\begin{aligned}
H_{1,V} &= -\frac{2m_H\left(\sqrt{2}G_F\right)^{1/2}r}{r-s}\\
&g_V\left(1+\hat{\alpha}_1^{\mathrm{eff}}-\frac{\kappa}{r}\hat{\alpha}_{ZZ}-\frac{\kappa}{2r}\frac{Q_l\,g_{em}(r-s)}{s\,g_V}\hat{\alpha}_{AZ}\right),\\
H_{1,A} &= \frac{2m_H\left(\sqrt{2}G_F\right)^{1/2}r}{r-s}g_A\left(1+\hat{\alpha}_2^{\mathrm{eff}}-\frac{\kappa}{r}\hat{\alpha}_{ZZ}\right),\\
H_{2,V} &= -\frac{2m_H\left(\sqrt{2}G_F\right)^{1/2}}{r-s}g_V\left(2\hat{\alpha}_{ZZ}-\frac{Q_l\,g_{cm}\,(r-s)}{s\,g_V}\hat{\alpha}_{AZ}\right),\\
H_{2,A} &= \frac{4m_H\left(\sqrt{2}G_F\right)^{1/2}}{r-s}g_A\,\hat{\alpha}_{ZZ}\,,\\
H_{3,V} &= -\frac{2m_H\left(\sqrt{2}G_F\right)^{1/2}}{r-s}g_V\left(2\hat{\alpha}_{Z\tilde{Z}}+\frac{Q_l\,g_{em}(r-s)}{s\,g_V}\hat{\alpha}_{A\tilde{Z}}\right),\\
H_{3,A} &= \frac{4m_H\left(\sqrt{2}G_F\right)^{1/2}}{r-s}g_A\,\hat{\alpha}_{Z\tilde{Z}}.
\end{aligned} \tag{B2}$$

Appendix C

As mentioned in the Sect. 6. Some conversion are useful to compare with other study.

In the previous CEPC CP study [23], the CP violation parameter $\tilde{g}$ can reach the limit of $[-0.04, 0.01]$ by using the CPV Lagrangian as following:

$$\begin{aligned}
\mathcal{L}_{HZZ} = &-\frac{1}{4}g_1 Z_{\mu v}Z^{\mu v}h-g_2 Z_v\partial_\mu Z^{\mu v}h\\
&+g_3 Z_\mu Z^\mu h-\frac{1}{4}\tilde{g}Z_{\mu v}\tilde{Z}^{\mu v}h,
\end{aligned} \tag{C1}$$

in this function, $g_0 = eM_Z/\left(c_w s_w\right)$ is the HZZ coupling in the Standard Model. Taking the convention of [36], g_3 is a small number in units of g_0, while $g_1, g_2, \tilde{g}$ are small numbers in units of $e^2/\left(g_0 s_w^2 c_w^4\right)$, so that the interaction is consistent with the dimension of mass.

In order to compare with this results. We can use the equations here:

$$\frac{H}{v}\tilde{c}_{ZZ}\frac{g_1^2+g_2^2}{4}Z_{\mu v}\tilde{Z}^{\mu v} = \frac{1}{4}\tilde{g}Z_{\mu v}\tilde{Z}^{\mu v}h, \tag{C2}$$

while $\tilde{g}$ is the number in units of $e^2/\left(g_0 s_w^2 c_w^4\right)$. So we can easily reach the limit of $\tilde{g}$ to $-0.013 \sim 0.013$ at 68% confidence level with 5.6 ab^{-1} in our study, this is a better result than the previous CEPC CP result [23].

In CLIC study [22], the best 95% C.L. limits on CP-violating couplings $\tilde{c}_{HW}$ and $\tilde{c}_{HB}$ are $[-7.0 \times 10^{-3}; 7.0 \times 10^{-3}]$ and $[-3.0 \times 10^{-2}; 3.0 \times 10^{-2}]$, respectively.

The SM EFT Lagrangian containing the Wilson coefficients in the SILH basis of dimension-6 CP-violating operators can be defined in terms of the mass eigenstates after

electroweak symmetry breaking (Higgs boson, W, Z, photon, etc.) as follows:

$$\mathcal{L}_{CPV} = -\frac{1}{4}\tilde{g}_{hgg}G^a_{\mu v}\tilde{G}^{\mu v}h - \frac{1}{4}\tilde{g}_{h\gamma\gamma}F_{\mu v}\tilde{F}^{\mu v}h - \frac{1}{4}\tilde{g}_{hzz}Z_{\mu v}\tilde{Z}^{\mu v}h - \frac{1}{2}\tilde{g}_{h\gamma z}Z_{\mu v}\tilde{F}^{\mu v}h - \frac{1}{2}\tilde{g}_{hww}W^{\mu v}\tilde{W}^{\dagger}_{\mu v}h, \tag{C3}$$

where $W_{\mu v}$, $Z_{\mu v}$ and $F_{\mu v}$ are the field strength tensors of W-boson, Z-boson and photon, respectively.

The relations between Lagrangian parameters in the mass basis [22] and in the gauge basis (Eq.(C3)) are as following:

$$\begin{aligned}\tilde{g}_{hzz} &= \frac{2g}{c_W^2 m_W}\left[\tilde{c}_{HB}s_W^2 - 4\tilde{c}_\gamma s_W^4 + c_W^2\tilde{c}_{HW}\right],\\ \tilde{g}_{h\gamma z} &= \frac{gs_W}{c_W m_W}\left[\tilde{c}_{HW} - \tilde{c}_{HB} + 8\tilde{c}_\gamma s_W^2\right].\end{aligned} \tag{C4}$$

Comparing Eqs. (15) and (C3), the connections of the *CP*-odd related parameters between the two equations are obvious:

$$\begin{aligned}\frac{1}{4}\tilde{g}_{hzz}Z_{\mu v}\tilde{Z}^{\mu v}h &= \frac{H}{v}\tilde{c}_{ZZ}\frac{g_1^2+g_2^2}{4}Z_{\mu v}\tilde{Z}^{\mu v},\\ \frac{1}{2}\tilde{g}_{hz\gamma}Z_{\mu v}\tilde{F}^{\mu v}h &= \frac{H}{v}\tilde{c}_{Z\gamma}\frac{e\sqrt{g_1^2+g_2^2}}{2}Z_{\mu v}\tilde{A}^{\mu v}.\end{aligned} \tag{C5}$$

Converted with the Eq. (C5), the 2σ bounds on $\tilde{c}_{Z_\gamma}$ and $\tilde{c}_{ZZ}$ are $[-0.36, 0.36]$ and $[-0.24, 0.24]$ respectively in CLIC study.

For other more study, we can also compare the Lagrangian they used in a similar way to get the comparable results.

References

1. G. Aad et al. (ATLAS), Observation of a new particle in the search for the Standard Model Higgs boson with the ATLAS detector at the LHC. Phys. Lett. B **716**, 1 (2012). arXiv:1207.7214 [hep-ex]
2. S. Chatrchyan et al. (CMS), Observation of a new boson at a mass of 125 GeV with the CMS experiment at the LHC. Phys. Lett. B **716**, 30 (2012). arXiv:1207.7235 [hep-ex]
3. G. Aad et al. (ATLAS), Study of the spin and parity of the Higgs boson in diboson decays with the ATLAS detector. Eur. Phys. J. C **75**, 476 (2015). arXiv:1506.05669 [hep-ex]
4. G. Aad et al. (ATLAS), Test of CP Invariance in vector-boson fusion production of the Higgs boson using the optimal observable method in the ditau decay channel with the ATLAS detector. Eur. Phys. J. C **76**, 658 (2016). arXiv:1602.04516 [hep-ex]
5. M. Aaboud et al. (ATLAS), Measurement of the Higgs boson coupling properties in the $H \to ZZ^* \to 4\ell$ decay channel at $\sqrt{s}$ = 13 TeV with the ATLAS detector. JHEP **03**, 095. arXiv:1712.02304 [hep-ex]
6. M. Aaboud et al. (ATLAS), Measurements of Higgs boson properties in the diphoton decay channel with 36 fb^{-1} of pp collision data at $\sqrt{s} = 13$ TeV with the ATLAS detector. Phys. Rev. D **98**, 052005 (2018). arXiv:1802.04146 [hep-ex]
7. V. Khachatryan et al. (CMS), Combined search for anomalous pseudoscalar HVV couplings in VH(H $\to b\bar{b}$) production and H $\to$ VV decay. Phys. Lett. B **759**, 672 (2016). arXiv:1602.04305 [hep-ex]
8. A.M. Sirunyan et al. (CMS), Measurements of the Higgs boson width and anomalous HVV couplings from on-shell and off-shell production in the four-lepton final state. Phys. Rev. D **99**, 112003 (2019). arXiv:1901.00174 [hep-ex]
9. A.M. Sirunyan et al. (CMS), Constraints on anomalous HVV couplings from the production of Higgs bosons decaying to τ lepton pairs. Phys. Rev. D **100**, 112002 (2019). arXiv:1903.06973 [hep-ex]
10. G. Aad et al. (ATLAS), CP properties of higgs boson interactions with top quarks in the $t\bar{t}H$ and tH processes using $H \to \gamma\gamma$ with the ATLAS detector. Phys. Rev. Lett. **125**, 061802 (2020). arXiv:2004.04545 [hep-ex]
11. A.M. Sirunyan et al. (CMS), Measurements of $t\bar{t}H$ production and the CP structure of the Yukawa interaction between the Higgs boson and top quark in the diphoton decay channel. Phys. Rev. Lett. **125**, 061801 (2020). arXiv:2003.10866 [hep-ex]
12. M. Cepeda et al., Report from Working Group 2: Higgs physics at the HL-LHC and HE-LHC, CERN Yellow Rep. Monogr. **7**, 221 (2019). arXiv:1902.00134 [hep-ph]
13. T. Behnke, J.E. Brau, P.N. Burrows, J. Fuster, M. Peskin, M. Stanitzki, Y. Sugimoto, S. Yamada, H. Yamamoto, The international linear collider technical design report, Tech. Rep. (Geneva, 2013). arXiv:1306.6329
14. A. Abada et al., (FCC), FCC-ee: the lepton collider: future circular collider conceptual design report volume 2. Eur. Phys. J. ST **228**, 261 (2019)
15. M.J. Boland et al. (CLIC, CLICdp), Updated baseline for a staged Compact Linear Collider (2016). arXiv:1608.07537 [physics.acc-ph]
16. M. Ahmad et al., CEPC-SPPC preliminary conceptual design report. 1. Physics and Detector (2015)
17. A.V. Gritsan et al., Snowmass white paper: prospects of CP-violation measurements with the Higgs boson at future experiments (2022). arXiv:2205.07715 [hep-ex]
18. I. Božović-Jelisavucić, N. Vukausinović, and D. Jeans, Measuring the CP properties of the Higgs sector at electron-positron colliders (2022). arXiv:2203.06819 [hep-ex]
19. A. Drutskoy, International Linear Collider (ILC), 2053-2571 (Morgan & Claypool Publishers, 2018)
20. T.A. Jovin, I.B. Jelisavcic, I. Smiljanic, G. Kacarevic, N. Vukasinovic, G.M. Dumbelovic, J. Stevanovic, M. Radulovic, D. Jeans, Probing the CP properties of the Higgs sector at ILC, in *International Workshop on Future Linear Colliders* (2021). arXiv:2105.06530 [hep-ph]
21. T. Ogawa, J. Tian, K. Fujii, Sensitivity to anomalous ZZH couplings at the ILC, PoS **EPS-HEP2017**, 322 (2017). arXiv:1712.09772 [hep-ex]
22. O. Karadeniz, A. Senol, K.Y. Oyulmaz, H. Denizli, CP-violating Higgs-gauge boson couplings in $H\nu\bar{\nu}$ production at three energy stages of CLIC. Eur. Phys. J. C **80**, 229 (2020). arXiv:1909.08032 [hep-ph]
23. H.-D. Li, C.-D. Lü, L.-Y. Shan, Sensitivity study of anomalous HZZ couplings at a future Higgs factory. Chin. Phys. C **43**, 103001 (2019). arXiv:1901.10218 [hep-ex]
24. W. Bernreuther, L. Chen, I. García, M. Perelló, R. Poeschl, F. Richard, E. Ros, M. Vos, CP-violating top quark couplings at future linear e^+e^- colliders. Eur. Phys. J. C **78**, 155 (2018). arXiv:1710.06737 [hep-ex]
25. B.L. Ioffe, V.A. Khoze, What can be expected from experiments on colliding e+ e- beams with e approximately equal to 100-GeV? Sov. J. Part. Nucl. **9**, 50 (1978)

26. B. Grzadkowski, M. Iskrzynski, M. Misiak, J. Rosiek, Dimension-six terms in the standard model Lagrangian. JHEP **10**, 085. arXiv:1008.4884 [hep-ph]
27. M. Beneke, D. Boito, Y.-M. Wang, Anomalous Higgs couplings in angular asymmetries of $H \to Z\ell^+\ell^-$ and e$^+$ e$^-$ $\to HZ$. JHEP **11**, 028. arXiv:1406.1361 [hep-ph]
28. N. Craig, J. Gu, Z. Liu, K. Wang, Beyond Higgs couplings: probing the Higgs with angular observables at future e^+e^- colliders. JHEP **03**, 050. arXiv:1512.06877 [hep-ph]
29. M. Davier, L. Duflot, F. Le Diberder, A. Rouge, The optimal method for the measurement of tau polarization. Phys. Lett. B **306**, 411 (1993)
30. W. Kilian, T. Ohl, J. Reuter, WHIZARD: simulating multi-particle processes at LHC and ILC. Eur. Phys. J. C **71**, 1742 (2011). arXiv:0708.4233 [hep-ph]
31. X. Mo, G. Li, M.-Q. Ruan, X.-C. Lou, Physics cross sections and event generation of e^+e^- annihilations at the CEPC. Chin. Phys. C **40**, 033001 (2016). arXiv:1505.01008 [hep-ex]
32. Y. Bai, C. Chen, Y. Fang, G. Li, M. Ruan, J.-Y. Shi, B. Wang, P.-Y. Kong, B.-Y. Lan, Z.-F. Liu, Measurements of decay branching fractions of $H \to b\bar{b}/c\bar{c}/gg$ in associated $(e^+e^-/\mu^+\mu^-)H$ production at the CEPC. Chin. Phys. C **44**, 013001 (2020). arXiv:1905.12903 [hep-ex]
33. M. Cacciari, G.P. Salam, G. Soyez, FastJet User Manual. Eur. Phys. J. C **72**, 1896 (2012). arXiv:1111.6097 [hep-ph]
34. M. Oreglia, A study of the reactions $\psi' \to \gamma\gamma\psi$, Other thesis (1980)
35. H. Cheng et al. (CEPC Physics Study Group), The Physics potential of the CEPC. Prepared for the US Snowmass Community Planning Exercise (Snowmass 2021), in 2022 Snowmass Summer Study (2022). arXiv:2205.08553 [hep-ph]
36. A. Alloul, B. Fuks, V. Sanz, Phenomenology of the Higgs Effective Lagrangian via FEYNRULES. JHEP **04**, 110. arXiv:1310.5150 [hep-ph]